Electronic Supplementary Material (ESI) for Physical Chemistry Chemical Physics.

Supporting information

Solution Self-Assembly Behavior of Rod-*alt*-Coil Alternating Copolymers via Simulation

Shanlong Li [1], *Ke Li* [1], *Qingsong Xu* [1], *Yuling Wang* [1], *Chunyang Yu* [1*], *Yongfeng Zhou* [1*]

[1]School of Chemistry & Chemical Engineering, Shanghai Key Laboratory of Electrical Insulation and Thermal Aging , State Key Laboratory of Metal Matrix Composites, Shanghai Jiao Tong University, 800 Dongchuan Road, Shanghai, China, 200240.

1. **DPD fundamentals.**
2. **The generation of the DPD model of rod-*alt*-coil ACPs.**
3. **Effects of k_0 on the rigidity of the rod chains.**
4. **Justification of simulation time.**
5. **Reproducibility of the simulation results.**
6. **Elimination of the finite size effect.**
7. **The formation of BCMs and PMs.**
8. **The definition and criteria of the loop and bridge conformations.**
9. **Rod alignment and orientation in the membrane obtained from $(R_6C_2)_6$.**
10. **Effects of coil length of the self-assembly of rod-*alt*-coil ACPs.**
11. **The calculation of π-π interaction.**
12. **The effect of π-π strength on the rod alignment.**
13. **The effect of MW and MWD.**
14. **Polydisperse systems.**
15. **Molecular packing behaviors of $(R_6C_3)_n$ in the monolayers of membrane.**
16. **Packing parameters.**
17. **Formation of unimolecular cylindrical micelle and disk.**
18. **References.**

1. DPD fundamentals.

In DPD method, like molecular dynamics, the motion of all the DPD beads obeys Newton's equation of motion.

$$\frac{d\boldsymbol{r}_i}{dt} = \boldsymbol{v}_i \ , \qquad \frac{d\boldsymbol{v}_i}{dt} = \boldsymbol{f}_i/m_i \tag{S1}$$

where $\boldsymbol{r}_i$, $\boldsymbol{v}_i$ and m_i denote the position vector, velocity vector and mass of beads respectively, and $\boldsymbol{f}_i$ is the force acting on bead i. The force $\boldsymbol{F}_{ij}$ exerted on bead i by bead j is consisted of a conservative force $\boldsymbol{F}_{ij}^C$, a dissipative force $\boldsymbol{F}_{ij}^D$ and a random force $\boldsymbol{F}_{ij}^R$. Thus, the total force $\boldsymbol{f}_i$ is given by

$$\boldsymbol{f}_i = \sum_{j \neq i} \left(\boldsymbol{F}_{ij}^C + \boldsymbol{F}_{ij}^D + \boldsymbol{F}_{ij}^R \right) \tag{S2}$$

where the sum runs over all other beads within the cutoff radius r_c. And the conservative force $\boldsymbol{F}_{ij}^C$, dissipative force $\boldsymbol{F}_{ij}^D$ and random force $\boldsymbol{F}_{ij}^R$ are given by

$$\boldsymbol{F}_{ij}^C = \begin{cases} a_{ij}\left(r_c - r_{ij}\right)\boldsymbol{e}_{ij} & r_{ij} \leq r_c \\ 0 & r_{ij} > r_c \end{cases} \tag{S3}$$

$$\boldsymbol{F}_{ij}^D = -\gamma \omega^D\left(r_{ij}\right)\left(\boldsymbol{e}_{ij} \cdot \boldsymbol{v}_{ij}\right)\boldsymbol{e}_{ij} \tag{S4}$$

$$\boldsymbol{F}_{ij}^R = \sigma \omega^R\left(r_{ij}\right)\theta_{ij}\boldsymbol{e}_{ij} \tag{S5}$$

where a_{ij} is a constant that describes the maximum repulsion between two interacting beads. r_{ij} is the distance between beads i and j. $\boldsymbol{e}_{ij} = \boldsymbol{r}_{ij}/r_{ij}$, $\boldsymbol{v}_{ij} = \boldsymbol{v}_i - \boldsymbol{v}_j$, $\boldsymbol{v}_i$ and $\boldsymbol{v}_j$ are the velocities of beads i and j, respectively. γ and σ are the amplitudes of dissipative and random forces, respectively. θ_{ij} is a randomly fluctuating variable. ω^D and ω^R are r-dependent weight functions for dissipative and random forces, respectively. According to the fluctuation-dissipation theorem, $\omega_{ij}^D(r)=[\omega_{ij}^R(r)]^2$ and $\sigma^2=2\gamma k_B T$ (σ=3 and γ=4.5). The following simple form of ω^D and ω^R was chosen by Groot and Warren[1]:

$$\omega^D(r) = [\omega^R(r)]^2 = \begin{cases} (1 - r/r_c)^2 & r \leq r_c \\ 0 & r > r_c \end{cases} \tag{S6}$$

2. The generation of the DPD model of rod-*alt*-coil ACPs.

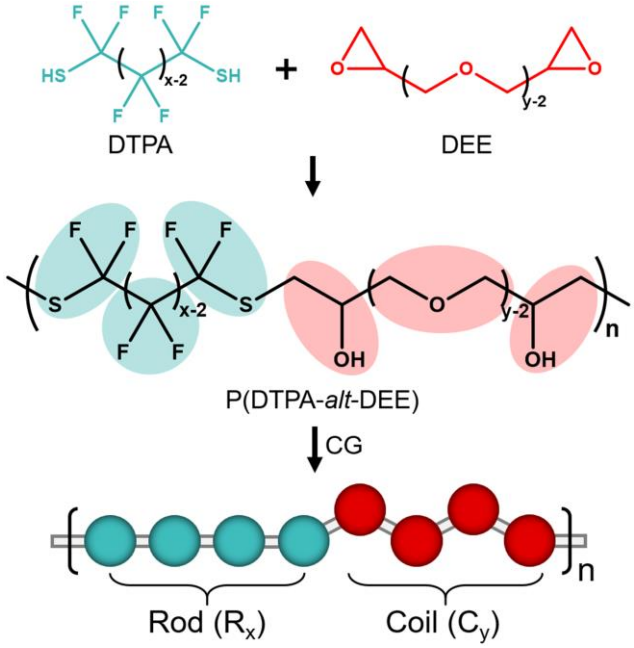

Fig. S1. P(DTPA-*alt*-DEE) serves as an example to illustrate the formation of the general DPD model of rod-*alt*-coil ACPs ($(R_xC_y)_n$). The cyan and red ellipses indicate the coarse-grained scheme. Cyan and red beads represent the solvophobic rod segments (R_x) and solvophilic coil segments (C_y), respectively.

3. Effects of k_θ on the rigidity of the rod chains.

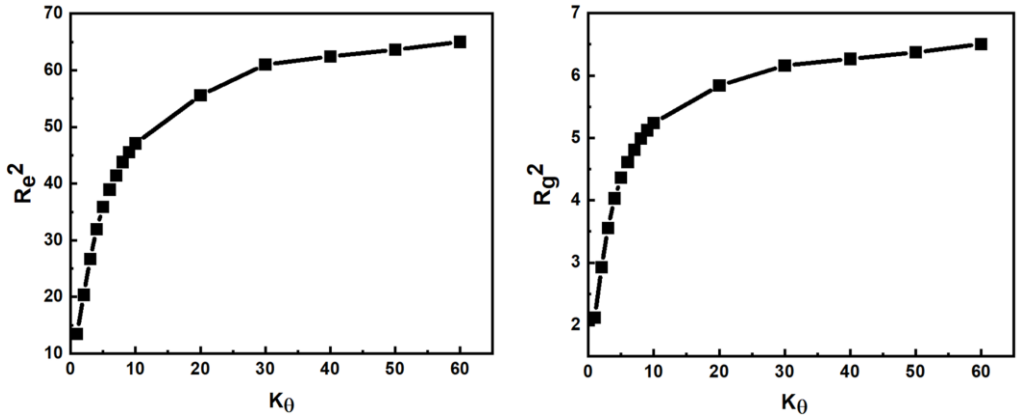

Fig. S2. Variation of the mean square end-to-end distance (R_e^2) and the mean square radius of gyration (R_g^2) with the rigidity k_θ of the rod chains.

4. Justification of simulation time.

A representative variation of the potential energy with simulation time is plotted in Figure S3, in which we can found that the simulation time is long enough for the system to reach equilibrium. In addition, through tracking the moving of polymer chains, our final simulation time is adequately long to have a polymer chain move on average more than ten times its radius of gyration. It reveals that the polymers have forgot their initial configuration and have completely relaxed.

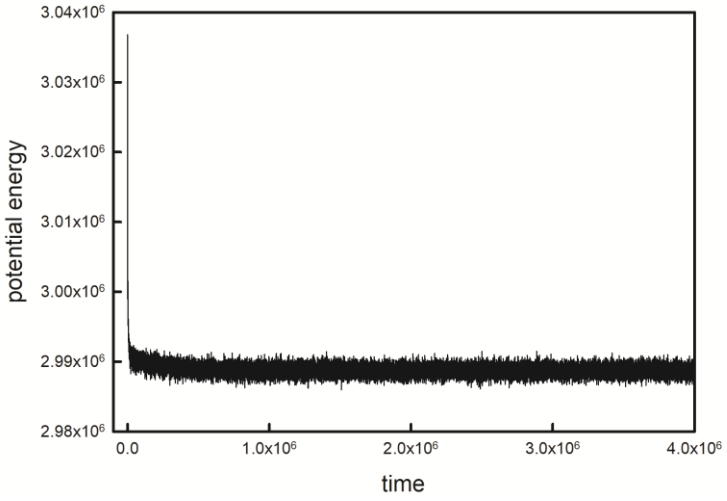

Fig. S3. Variation of potential energy with the simulation time in the self-assembly of $(R_6C_5)_6$ as a representative example.

Table S1. Diffusion coefficient (D), the average distance one chain moves in 4.0×10^5 time steps (d_{move}), the radius of gyration of the chain (R_g), and the ratio between d_{move} and R_g.

Polymers	D	d_{move}	R_g	d_{move}/R_g
$(R_{10}C_{12})_6$	7.91×10^{-4}	43.57	7.20	6.05
$(R_8C_8)_6$	8.85×10^{-4}	46.09	5.39	8.55
$(R_5C_5)_6$	1.03×10^{-3}	49.72	3.67	13.55

5. Reproducibility of the simulation results.

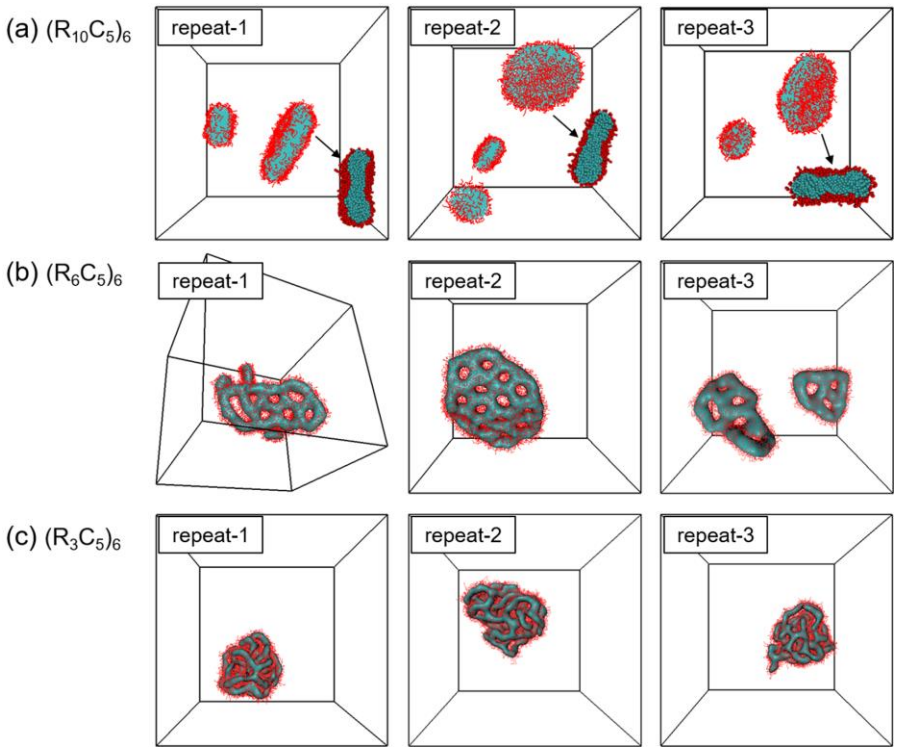

Fig. S4. The results of three times repeat simulation of polymer $(R_{10}C_5)_6$, $(R_6C_5)_6$, and $(R_3C_5)_6$, respectively. Rod and coil segments are denoted as cyan and red, respectively.

6. Elimination of the finite size effect.

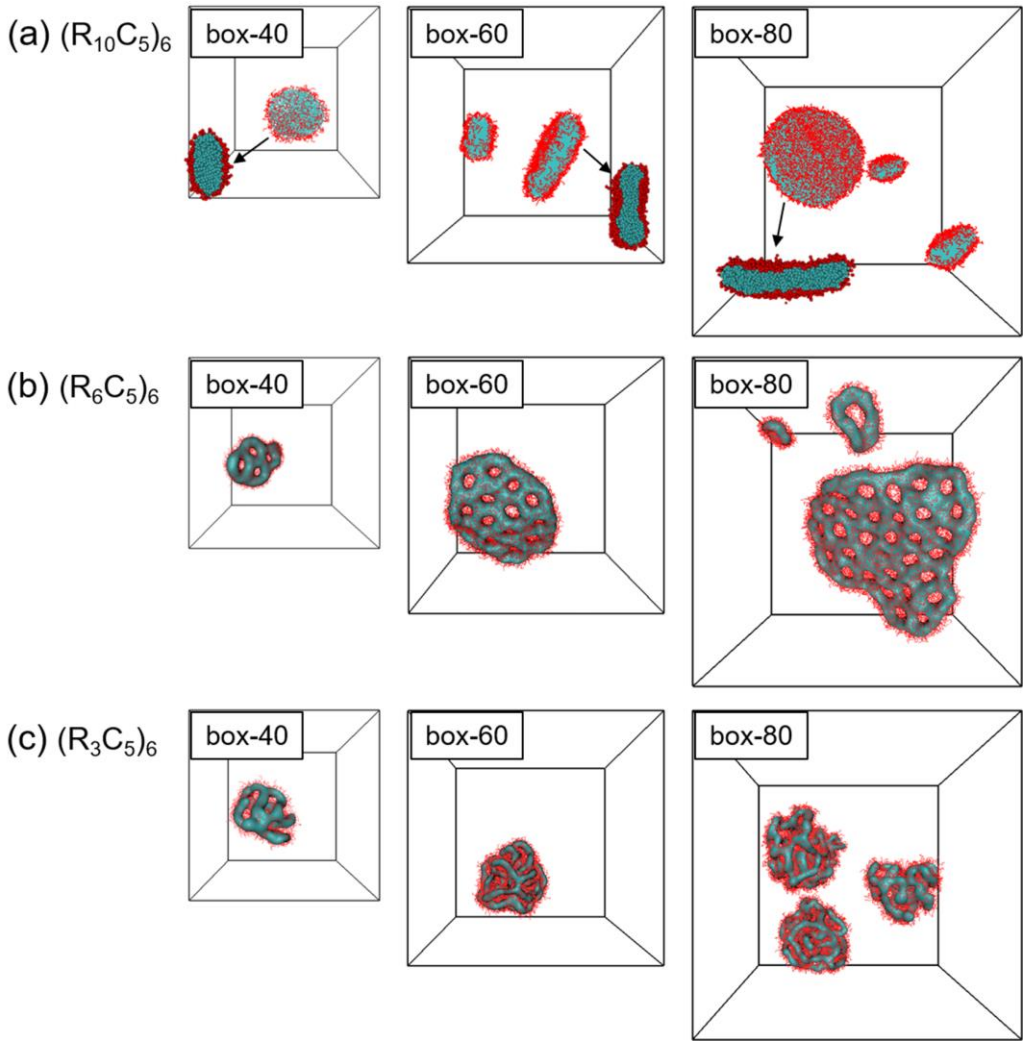

Fig. S5. The simulation results with different box sizes for polymer $(R_{10}C_5)_6$, $(R_6C_5)_6$, and $(R_3C_5)_6$, respectively. Rod and coil segments are denoted as cyan and red, respectively.

7. The formation of BCMs and PMs.

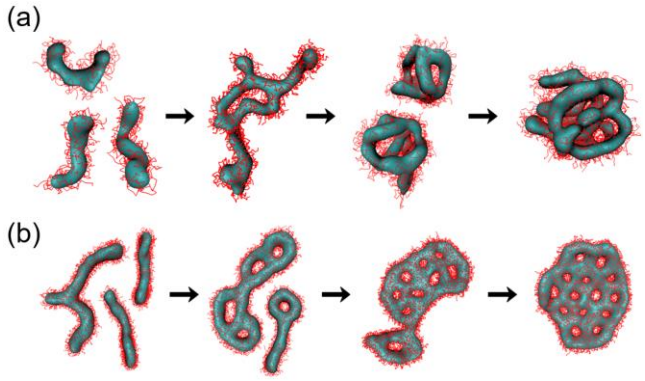

Fig. S6. Sequential snapshots illustrated for the formation of BCMs (a) and PMs (b). Rod and coil segments are denoted as cyan and red, respectively.

8. The definition and criteria of the loop and bridge conformations.

As shown in Figure S6, -ABA- is a part of the polymer chain. The centers of mass of the segments are denoted as $\boldsymbol{r}_{A1}$, $\boldsymbol{r}_{B}$ and $\boldsymbol{r}_{A2}$. Two vectors ($\boldsymbol{v}_1$, $\boldsymbol{v}_2$) can be obtained, as well as the angle between vectors (φ). The quantity of interest is given as

$$\cos\varphi = \frac{(\boldsymbol{r}_{A1} - \boldsymbol{r}_{B}) \cdot (\boldsymbol{r}_{A2} - \boldsymbol{r}_{B})}{|\boldsymbol{r}_{A1} - \boldsymbol{r}_{B}||\boldsymbol{r}_{A2} - \boldsymbol{r}_{B}|}$$

Using this quantity, the segment is defined as loop conformation if $\cos\varphi > 0$, while bridge conformation if $\cos\varphi < 0$. Through counting the numbers of loop segments (N_L) and bridge segments (N_B), the percentage of the bridge conformations (ν_{bridge}) can be given as $\nu_{bridge} = N_B/(N_B+N_L)$.

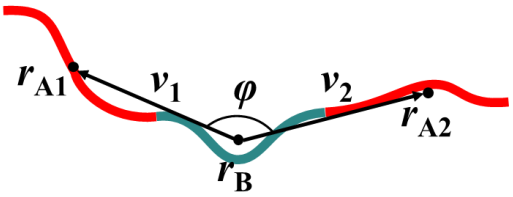

Fig. S7. Scheme for calculating the conformation of the repeating segments.

9. Rod alignment and orientation in the membrane obtained from $(R_6C_2)_6$.

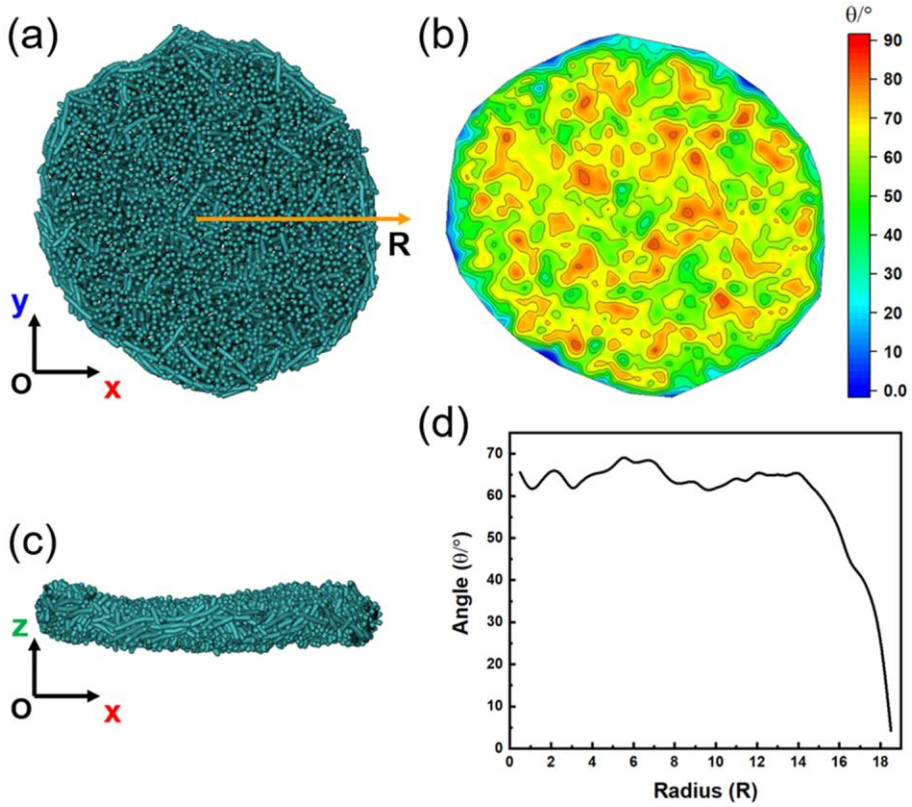

Fig. S8. Rod alignment and orientation in the membrane obtained from $(R_6C_2)_6$. (a) Top view of the membrane; (b) Angle distribution in the XOY plane of the membrane; (c) Side view of the membrane; (d) Angle distribution along the radial direction (R) of the membrane. θ is the included angle between rod and XOY plane, while "Radius" is the distance between rods and the center of mass of membrane. Coil segments are omitted for clarity.

10. Effects of coil length of the self-assembly of rod-*alt*-coil ACPs.

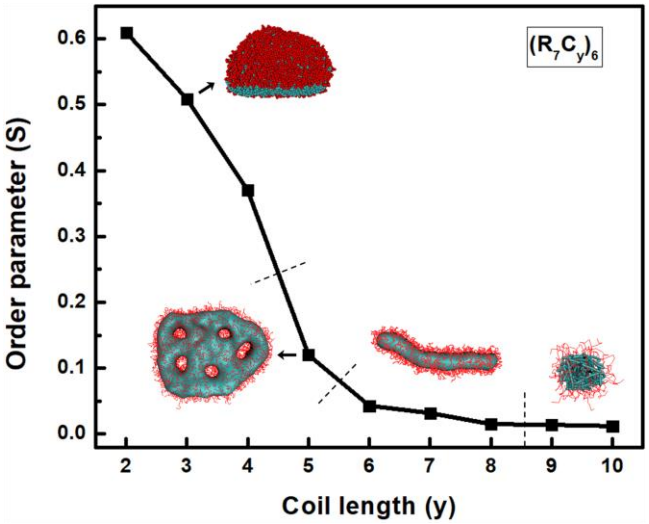

Fig. S9. Variations of the order parameter (S) as a function of the coil length (x) for $(R_7C_y)_6$. Insets show the corresponding snapshots. Rod and coil segments are denoted as cyan and red, respectively.

11. The calculation of π-π interaction.

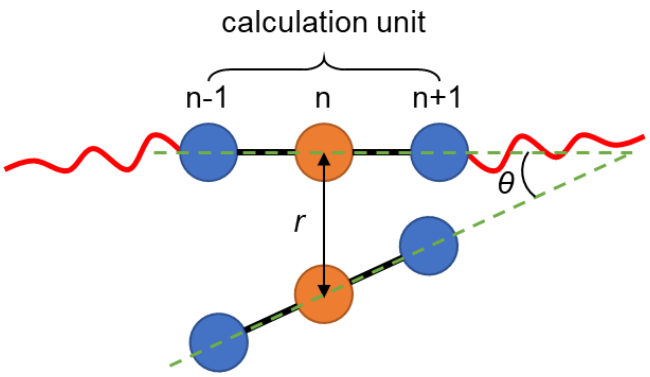

Fig. S10. Scheme for the calculation of π-π interaction between rod segments.

The pi-pi interaction is calculated as follows:

$$\begin{aligned} V_{\pi-\pi}(r,\theta) &= -\epsilon\cos^2\theta(1-r) \quad r < r_{cut} \\ &= 0 \quad r < r_{cut} \end{aligned}$$

where ϵ is the strength. As shown in Fig. S10, every three neighboring particles in the rod segments are a calculation unit. π-π interaction between two units is acted on the center particle (yellow bead), and r is the distance of two center particles. The vector from particle n-1 to n+1 is defined as the vector of this unit. The angle θ between two units is the included angle of their vectors.

Detailed information can be found in the website of this software:

1. https://galamost.readthedocs.io/en/latest/forcefield-nonbonded.html#linear-pi-pi
2. https://bitbucket.org/galamostdevelopergroup/source-code/src/master/src/lib_code/cuda/CenterForce.cu
3. https://galamost.ciac.jl.cn

12. The effect of π-π strength on the rod alignment.

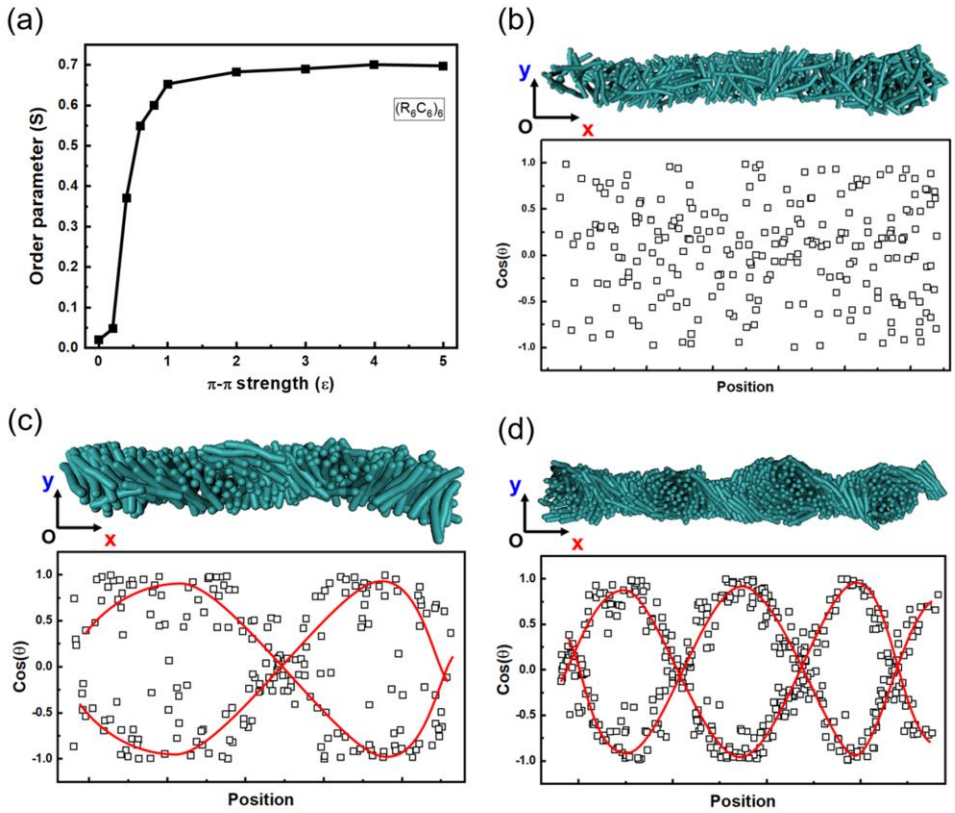

Fig. S11. (a) Variation of the order parameter (*S*) as a function of π-π strength (ε) for $(R_6C_6)_6$. (b-d) Rod alignment and orientation in the cylindrical micelles with ε = 0, 0.4 and 1.0, respectively. θ is the included angle between rod and OX axis, while "Position" is the center of mass of the rod along the OX direction. Coil segments are omitted for clarity. Rod and coil segments are denoted as cyan and red, respectively.

13. The effect of MW and MWD.

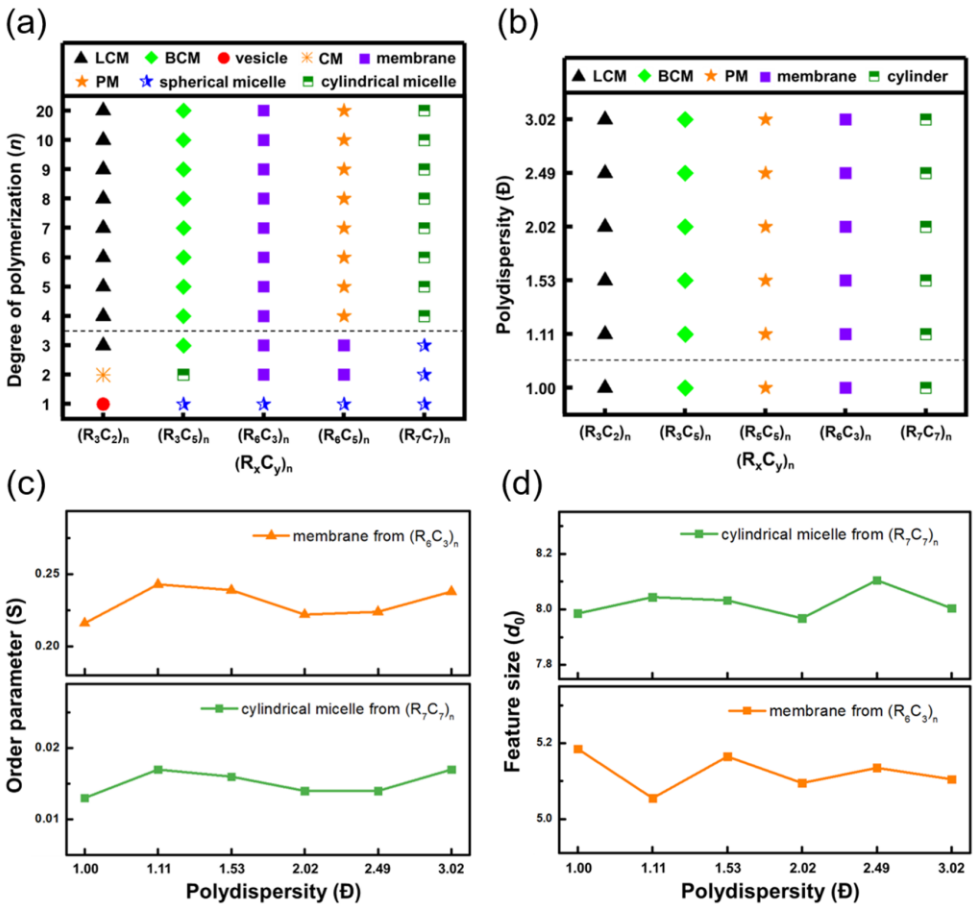

Fig. S12. (a) Effect of degree of polymerization on the morphologies of $(R_3C_2)_n$, $(R_3C_5)_n$ $(R_6C_3)_n$, $(R_6C_5)_n$ and $(R_7C_7)_n$. (b) Effect of polymer polydispersity on the morphologies of $(R_3C_2)_n$, $(R_3C_5)_n$ $(R_5C_5)_n$, $(R_6C_3)_n$ and $(R_7C_7)_n$. (c) Effect of polymer polydispersity on the order parameters. (d) Effect of polymer polydispersity on the feature sizes.

14. Polydisperse systems.

Table S2. The polydisperse polymer systems (samples 1-6) with different polydispersity for simulations.

	n = 6	**n = 10**	**n = 20**	**n = 40**	**n = 60**	**n = 80**	$\mathbf{n_{average}}$	**Đ**
Sample 1	100%	0%	0%	0%	0%	0%	6.00	1.00
Sample 2	5%	5%	5%	75%	10%	0%	31.8	1.11
Sample 3	10%	30%	40%	10%	10%	0%	21.6	1.53
Sample 4	30%	30%	10%	10%	10%	10%	24.8	2.02
Sample 5	60%	10%	5%	5%	5%	15%	17.2	2.49
Sample 6	75%	5%	5%	5%	0%	10%	16.00	3.02

Note: The polydisperse polymer samples (samples 1-6) were obtained by mixing the alternating copolymers (n=6, 10, 20, 40, 60 and 80) with different volume ratios.

15. Molecular packing behaviors of $(R_6C_3)_n$ in the monolayers of membrane.

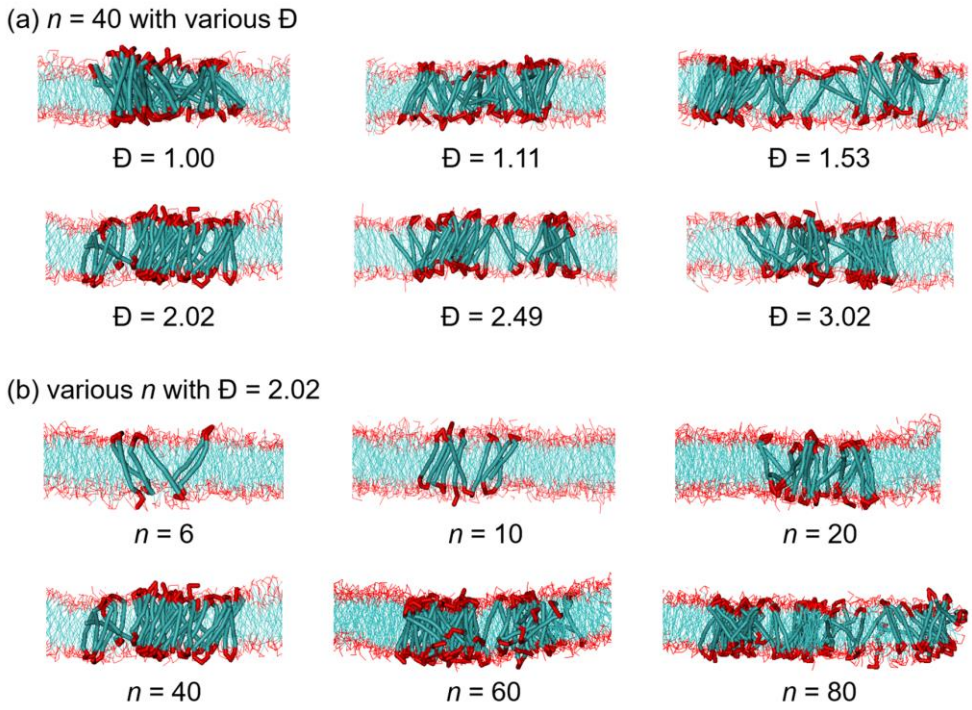

Fig. S13. (a) The packing model of $(R_6C_3)_{40}$ inside the membranes of different polydisperse systems. (b) The packing model of $(R_6C_3)_n$ with various *n* inside the membranes with Đ = 2.02. Rod and coil segments are denoted as cyan and red, respectively.

16. Packing parameters.

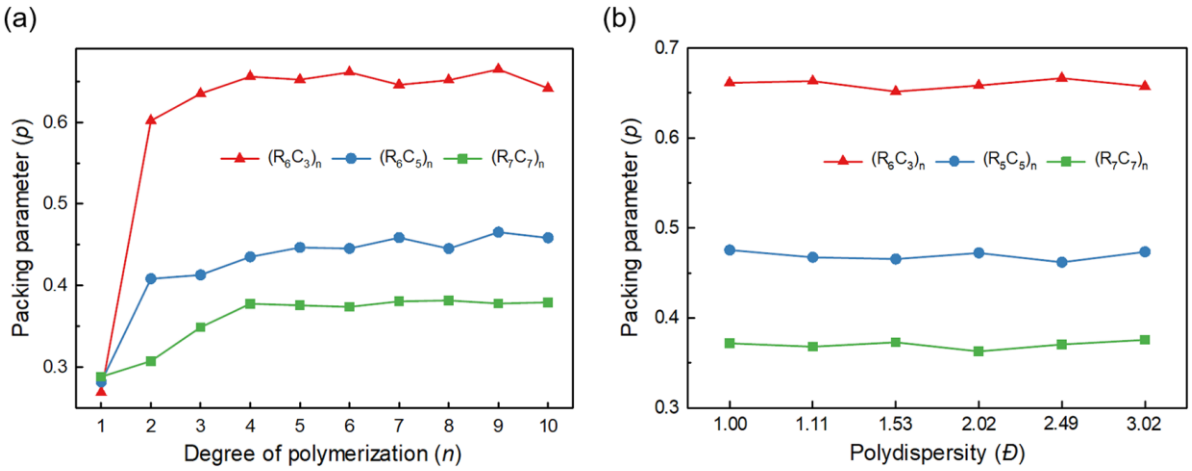

Fig. S14. (a) Variation of packing parameters as a function of degree of polymerization for $(R_6C_3)_n$, $(R_6C_5)_n$ and $(R_7C_7)_n$. (b) Variation of packing parameters as a function of polydispersity for $(R_6C_3)_n$, $(R_5C_5)_n$ and $(R_7C_7)_n$.

17. Formation of unimolecular cylindrical micelle and disk.

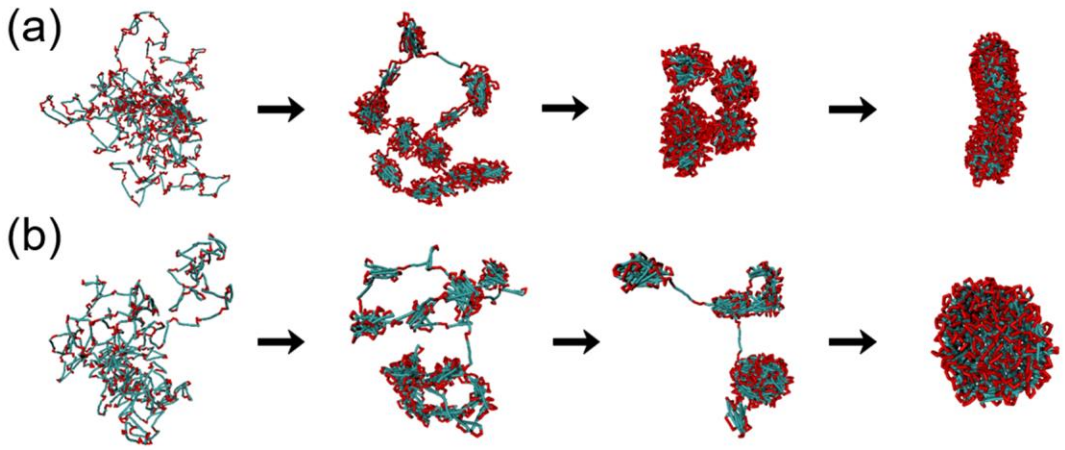

Fig. S15. Sequential snapshots for the formation of unimolecular cylindrical micelle from $(R_7C_7)_{200}$ (a) and unimolecular disk from $(R_6C_3)_{250}$ (b). Rod and coil segments are denoted as cyan and red, respectively.

References

(1) Groot, R. D.; Warren, P. B. Dissipative particle dynamics: Bridging the gap between atomistic and mesoscopic simulation. *J. Chem. Phys.* **1997,** *107*, 4423.